Applied Analysis and Optimization
Volume 8, Number 1, 2024, 71–85

Yokohama Publishers
ISSN 2189-1664 Online Journal

ON THE DYNAMICS AND CHAOS CONTROL OF A PERTURBED NEURON MODEL

AHMED MOHAMMED AHMED EL-SAYED, SANAA MOUSSA SALMAN, AND ALI MOHAMMED ALI ABO-BAKR

Abstract. The present study investigates the dynamical characteristics of a neuron model that is modified through parametric perturbation in the Rulkov map. Firstly, we conduct a local stability analysis and demonstrate that the system displays both flip and Neimark-Sacker bifurcations. In order to control chaos in the system, we apply the state feedback control method. The obtained theoretical results are validated through numerical simulations. Additionally, the effect of the perturbation parameter is illustrated via numerical simulations. Notably, a halving-period bifurcation occurs due to a small alteration in the perturbation parameter.

1. Introduction

The brain is a complex system that consists of millions of interconnected neurons with chemical and electrical synapses [21]. To understand the essential dynamics of neuron activities, various neuron models have been developed over time. These models can be categorized into two groups: conductance-dependent and conductance-independent neuron models [27]. Conductance-dependent models, such as Morris-Lecar [18], Hodgkin-Huxley [13], Wilson [25], and Chay models [5, 28], utilize electrophysiological features to mimic the neuron activity by rebuilding the ion channels [2-6]. Conductance-independent neuron models, on the other hand, like FitzHugh-Nagumo [9], Hindmarsh-Rose (HR) [12], Izhikevich [15], and Rulkov map models [20], are built on dynamical hypotheses and do not consider the neural physiological context [27]. Effective neural models play a crucial role in understanding key functions like decision-making, memory, and sensory information processing, as well as the development of artificial intelligent systems based on neuromorphic principles [2]. Among the available models, the Rulkov map-based neuron model which is given by [20]

$$\begin{aligned} x_{n+1} &= \frac{\alpha}{1+x_n^2} + y_n, \\ y_{n+1} &= y_n - \sigma(x_n - \rho), \end{aligned} \tag{1.1}$$

has received significant attention due to its simplicity and ability to capture neuronal dynamics discontinuity. The model has control parameters, namely α, σ, and ρ, which help simulate changes in the neuronal membrane potential represented by x_n [21, 24]. Although y_n holds no particular biological interpretation, it aids in grasping neuronal dynamics [3].
The Rulkov map-based neuron model displays rich nonlinear dynamics and notable

2020 *Mathematics Subject Classification.* 39A30, 39A28, 34H10,
Key words and phrases. Rulkov map, stability, bifurcations, Chaos.

biological neuronal features [4, 7, 14, 21–24]. A perturbation can create unexpected behavior in the Rulkov map-based neuron model, similar to the malfunctioning of the neuronal membrane due to pathologies. This perturbation can be represented by the equation [6]

$$\begin{aligned} x_{n+1} &= \frac{\alpha(1+b_n\epsilon)}{1+x_n^2} + y_n, \\ y_{n+1} &= y_n - \sigma(x_n - \rho), \end{aligned} \tag{1.2}$$

where ϵ is a perturbation parameter, b_n is a control parameter and the traditional Rulkov map (1.1) is obtained when $\epsilon = 0$.
This paper studies the dynamics of model (1.2) by investigating its fixed point, stability analysis, and bifurcation analysis in sections 2 and section 3, respectively. Section 4 applies state feedback control methods to achieve chaos control in the system (1.2). Ultimately, section 5 presents numerical simulations that confirm theoretical findings and illustrate the complex dynamics of the system (1.2).

2. Local stability analysis

The system (1.2) has the unique fixed point $(x^*, y^*) = (\rho, \rho - \frac{\alpha(1+b_n\epsilon)}{1+\rho^2})$ which is the solution of the following system

$$\begin{aligned} x &= \frac{\alpha(1+b_n\epsilon)}{1+x^2} + y, \\ y &= y - \sigma(x - \rho). \end{aligned}$$

The Jacobian matrix calculated at (x^*, y^*) reads

$$J(x^*, y^*) = \begin{pmatrix} \frac{-2\rho\alpha(1+b_n\epsilon)}{(1+\rho^2)^2} & 1 \\ -\sigma & 1 \end{pmatrix}.$$

The characteristic equation associated to the $J(x^*, y^*)$ is given by

$$\lambda^2 - tr(J)\lambda + det(J) = 0, \tag{2.1}$$

where $tr(J) = 1 - \frac{2\rho\alpha(1+b_n\epsilon)}{(1+\rho^2)^2}$ and $det(J) = \sigma - \frac{2\rho\alpha(1+b_n\epsilon)}{(1+\rho^2)^2}$.
To determine the local stability of the system (1.2) at the fixed point (x^*, y^*), the following lemma is a useful tool.

Lemma 2.1 ([1]). *Let $F(\lambda) = \lambda^2 + P\lambda + Q$. Suppose that $F(1) > 0$, and $F(\lambda) = 0$ has two roots λ_1 and λ_2. Then*

1. *$F(-1) > 0$ and $Q < 1$ if and only if $|\lambda_1| < 1$ and $|\lambda_2| < 1$;*
2. *$F(-1) < 0$ if and only if $|\lambda_1| < 1$ and $|\lambda_2| > 1$ (or $|\lambda_1| > 1$ and $|\lambda_2| < 1$);*
3. *$F(-1) > 0$ and $Q > 1$ if and only if $|\lambda_1| > 1$ and $|\lambda_2| > 1$;*
4. *$F(-1) = 0$ and $P \neq 0, 2$ if and only if $\lambda_1 = -1$ and $|\lambda_2| \neq 1$;*
5. *$P^2 - 4Q < 0$ and $Q = 1$ if and only if λ_1 and λ_2 are complex and $|\lambda_{1,2}| = 1$.*

Using the above Lemma we obtain the following result.

Proposition 2.2. *The fixed point $(x^*, y^*) = (\rho, \rho - \frac{\alpha(1+b_n\epsilon)}{1+\rho^2})$ is*

1. *a sink if* $\dfrac{(\sigma-1)(1+\rho^2)^2}{2\rho(1+b_n\epsilon)} < \alpha < \dfrac{(\sigma+2)(1+\rho^2)^2}{4\rho(1+b_n\epsilon)}$,
2. *a source if* $\alpha < \min\{\dfrac{(\sigma-1)(1+\rho^2)^2}{2\rho(1+b_n\epsilon)}\ ,\ \dfrac{(\sigma+2)(1+\rho^2)^2}{4\rho(1+b_n\epsilon)}\}$,
3. *a saddle if* $\alpha > \dfrac{(\sigma+2)(1+\rho^2)^2}{4\rho(1+b_n\epsilon)}$,
4. *a non-hyperbolic if* $\alpha = \dfrac{(\sigma+2)(1+\rho^2)^2}{4\rho(1+b_n\epsilon)}$, *and* $\dfrac{2\rho\alpha(1+b_n\epsilon)}{(1+\rho^2)^2} \neq 1, 3$.

3. Bifurcations analysis

The system (1.2) exhibits two types of bifurcations, namely flip bifurcation and Neimark-Sacker bifurcation, as we discuss in what follows.
We first discuss the flip bifurcation of (1.2) at (x^*, y^*). Suppose that $\lambda_{1,2}$, the two roots of equation (2.1), are real ,i.e.,

$$(\frac{2\rho\alpha(1+b_n\epsilon)}{(1+\rho^2)^2} - 1)^2 - 4(\sigma - \frac{2\rho\alpha(1+b_n\epsilon)}{(1+\rho^2)^2}) > 0. \tag{3.1}$$

Let

$$\alpha_F = \frac{(\sigma+2)(1+\rho^2)^2}{4\rho(1+b_n\epsilon)},$$

and

$$\frac{2\rho\alpha((1+b_n\epsilon))}{(1+\rho^2)^2} \neq 1, 3. \tag{3.2}$$

Then, from the previous proposition, $\lambda_1 = -1$ and $\lambda_2 \neq \pm 1$.
Let $\tilde{x}(n) = x(n) - x^*$ and $\tilde{y}(n) = y(n) - y^*$ to transform the fixed point (x^*, y^*) of the system (1.2) to the origin producing the following system

$$\begin{aligned} \tilde{x}(n+1) &= \frac{\alpha(1+b_n\epsilon)}{1+(\tilde{x}(n)+x^*)^2} + \tilde{y}(n) + y^* - x^*, \\ \tilde{y}(n+1) &= \tilde{y}(n) - \sigma\ \tilde{x}(n). \end{aligned} \tag{3.3}$$

Expanding (3.3) as a Taylor series at $(0,0)$ up to terms of order 3 produces the following system

$$\begin{aligned} \tilde{x}(n+1) =& a_{10}\tilde{x}(n) + a_{01}\tilde{y}(n) + a_{20}\tilde{x}(n)^2 + a_{30}\tilde{x}(n)^3 + O(\|X\|), \\ \tilde{y}(n+1) =& \tilde{y}(n) - \sigma\ \tilde{x}(n), \end{aligned} \tag{3.4}$$

where $a_{10} = \dfrac{-2\rho\alpha(1+b_n\epsilon)}{(1+\rho^2)^2}$, $a_{01} = 1$, $a_{20} = \dfrac{\alpha(1+b_n\epsilon)(3\rho^2-1)}{(1+\rho^2)^2}$, $a_{30} = \dfrac{2\alpha(1+b_n\epsilon)(1+\rho^2-24\rho^3)}{(1+\rho^2)^4}$ and $X = (\tilde{x}(n), \tilde{y}(n))^T$. System (3.4) can be rewritten as

$$\begin{pmatrix} \tilde{x}(n) \\ \tilde{y}(n) \end{pmatrix} \to J(x^*, y^*) \begin{pmatrix} \tilde{x}(n) \\ \tilde{y}(n) \end{pmatrix} + \begin{pmatrix} F_1(\tilde{x}(n), \tilde{y}(n), \sigma) \\ F_2(\tilde{x}(n), \tilde{y}(n), \sigma) \end{pmatrix}, \tag{3.5}$$

Where $F_1 = a_{20}\tilde{x}(n)^2 + a_{30}\tilde{x}(n)^3 + O(\|X\|)$ and $F_2 = 0$. It follows that

$$B_1(x,y) = \sum_{i,j=1}^{2} \frac{\partial^2 F_1(\zeta,\alpha)}{\partial\zeta_i\ \partial\zeta_j}\ |_{\zeta=0}\ x_i y_j = 2a_{20}x_1y_1,$$

$$B_2(x,y) = \sum_{i,j=1}^{2} \frac{\partial^2 F_2(\zeta,\alpha)}{\partial\zeta_i\ \partial\zeta_j}\ |_{\zeta=0}\ x_i y_j = 0,$$

$$C_1(x,y,u) = \sum_{i,j,k=1}^{2} \frac{\partial^3 F_1(\zeta,\alpha)}{\partial\zeta_i\ \partial\zeta_j\ \partial\zeta_k}\ |_{\zeta=0}\ x_i y_j u_k = 6a_{30}x_1y_1u_1,$$

$$C_2(x,y,u) = \sum_{i,j,k=1}^{2} \frac{\partial^3 F_2(\zeta,\alpha)}{\partial\zeta_i\ \partial\zeta_j\ \partial\zeta_k}\ |_{\zeta=0}\ x_i y_j u_k = 0,$$

and $\alpha = \alpha_F$.
Therefore, $B(x,y) = (B_1(x,y)\ B_2(x,y))^T$ and $C(x,y,u) = (C_1(x,y,u)\ C_2(x,y,u))^T$ are multilinear symmetric vector functions of $x, y, u \in \mathbb{R}^2$.
At $\alpha = \alpha_F$ the Jacobian matrix has an eigenvalue $\lambda_1 = -1$ with corresponding one-dimensional eigenspace spanned by an eigenvector $v \in \mathbb{R}^2$ such that $J(\alpha_F)v = -v$. Let $w \in R^2$ be the adjoint eigenvector ,i.e., $J^T(\alpha_F)w = -w$. By simple calculation we find that

$$v = (1\ 1 + \frac{2\rho\alpha(1+b_n\epsilon)}{(1+\rho^2)^2})^T,$$

$$w = (-2\ 1)^T.$$

To normalize w with respect to v, we denote

$$w = (\frac{-2(1+\rho^2)^2}{\sqrt{5}(2\rho\alpha(1+b_n\epsilon)-1)}\ \frac{(1+\rho^2)^2}{\sqrt{5}(2\rho\alpha(1+b_n\epsilon)-1)})^T.$$

We can see that $\langle v, w\rangle = 1$, where $\langle v, w\rangle = v_1w_2 + v_2w_1$,i.e., $\langle .,.\rangle$ is the standard scalar product in R^2.
The direction of the flip bifurcation is determined from the sign of the critical normal form coefficient $\eta(\alpha_F)$ which is given by the following formula

$$\eta(\alpha_F) = \frac{1}{6}\langle w, C(v,v,v)\rangle - \frac{1}{2}\langle w, B(v,(J-I)^{-1}B(v,v))\rangle.$$

From the above analysis and the bifurcation Theory in section 4 in [16](see also [10, 19, 26]), we deduce the following result.

Theorem 3.1. *If the conditions (3.1) and (3.2) hold and* $\alpha_F = \dfrac{(\sigma+2)(1+\rho^2)^2}{4\rho(1+b_n\epsilon)}$, *then system (1.2) exhibits a flip bifurcation at the fixed point* (x^*, y^*) *when the parameter* α *varies in a small neighborhood of* α_F. *In addition, if* $\alpha_F > 0$ *(respectively,* $\alpha_F < 0$*), then the period-2 orbits that bifurcate from* (x^*, y^*) *are stable (respectively, unstable).*

In what follows, we investigates the occurenc of a Neimark-Sacker bifurcation by using the Neimark-Sacker Theorem in [10, 16, 19, 26].
Suppose that the two roots of equation (2.1) are complex ,i.e.,

$$(1-\frac{2\rho\alpha(1+b_n\epsilon)}{(1+\rho^2)^2})^2-4(\sigma-\frac{2\rho\alpha(1+b_n\epsilon)}{(1+\rho^2)^2})<0. \tag{3.6}$$

Let

$$\frac{2\rho\alpha(1+b_n\epsilon)}{(1+\rho^2)^2}<3, \tag{3.7}$$

and

$$\alpha_{NS}=\frac{(\sigma-1)(1+\rho^2)^2}{2\rho(1+b_n\epsilon)}.$$

From Lemma 2.1 we deduce that at $\alpha=\alpha_{NS}$ the eigenvalues of the matrix associated with the linearization of the map (3.5) at $(\tilde{x},\tilde{y})=(0,0)$ are conjugate with modulus 1, and they can be written as

$$\lambda,\ \bar{\lambda}=\mu(\alpha_{NS})\pm i\omega(\alpha_{NS})=\frac{tr(J)}{2}\pm\frac{i}{2}\sqrt{4det(J)-(tr(J))^2}$$

and

$$|\lambda(\alpha_{NS})|=1,$$
$$\frac{d|\lambda(\alpha)|}{d\alpha}|_{\alpha=\alpha_{NS}}=\frac{-\rho(1+b_n\epsilon)}{(1+\rho^2)^2}\neq 0\ whenever\ \rho\neq 0.$$

Moreover, if $tr(J(\alpha_{NS}))\neq 0,-1$ i.e,

$$\frac{2\rho\alpha(1+b_n\epsilon)}{(1+\rho^2)^2}\neq 1,2, \tag{3.8}$$

then ,obviously, $\lambda^k(\alpha_{NS})\neq 1$ for $k=1,2,3,4$.
Let $v\in C^2$ be an eigenvector of $J(\alpha_{NS})$ which correspond to the eigenvalue $\lambda(\alpha_{NS})$ such that

$$J(\alpha_{NS})v=\lambda(\alpha_{NS})v,\ J(\alpha_{NS})v=\bar{\lambda}(\alpha_{NS})v.$$

suppose that $w\in C^2$ is an eigenvector of of the transposed matrix $J^T(\alpha_{NS})$ that corresponds to its eigenvalue, $\bar{\lambda}(\alpha_{NS})$,

$$J^T(\alpha_{NS})w=\bar{\lambda}(\alpha_{NS})w,\ J^T(\alpha_{NS})w=\lambda(\alpha_{NS})w.$$

direct computations yield

$$v\ \sim\ (1-\lambda\ 1+\frac{2\rho\alpha(1+b_n\epsilon)}{(1+\rho^2)^2})^T,$$
$$w\ \sim\ (1-\lambda\ -1)^T.$$

In order to normalize w with respect to q, let

$$w=\frac{1}{\gamma}(1-\lambda\ -1)^T,$$

where $\gamma=(1-\lambda)(\frac{2\rho\alpha(1+b_n\epsilon)}{(1+\rho^2)^2})$. We can see that $\langle v,w\rangle=1$, where $\langle v,w\rangle=\bar{v_1}w_2+\bar{v_2}w_1$, that is, $\langle .,.\rangle$ denotes standard scalar product in C^2.

Now, for any vector $X \in \mathbb{C}^2$, it can be expressed for α near α_{NS} as $X = z\,v + \bar{z}\bar{v}$, for some complex z. As a consequence, $z = \langle w, X\rangle$. Thus, system (3.5) can be transformed for sufficiently small $|alpha|$ (close to α_{NS}) into the following form:

$$z \mapsto \lambda(\alpha)z \ + \ g(z, \bar{z}, \sigma),$$

where $\lambda(\alpha)$ can be expressed as $\lambda(\alpha) = (1+\phi(\alpha))e^{i\theta(\alpha)}$, where $\phi(\alpha)$ is a smooth function with $\phi(\alpha_{NS}) = 0$ and g is a smooth function of $z, \bar{z}, \alpha$ whose Taylor expansion with respect to $z, \bar{z}$ includes quadratic and higher-order terms:

$$g(z, \bar{z}, \alpha) = \sum_{i,j\geq 2} \frac{1}{i!j!} g_{i,j}(\alpha)\ z^i\ \bar{z}^j,$$

where $g_{i,j} \in C$, $i, j = 1, 2.....$ Now, the Taylor coefficients $g_{i,j}$ can be represented as follows:

$$g_{20}(\alpha_{NS}) = \langle w,\ B(v, v)\rangle,\ g_{11}(\alpha_{NS}) = \langle w,\ B(v, \bar{v})\rangle,$$

$$g_{02}(\alpha_{NS}) = \langle w,\ B(\bar{v}, \bar{v})\rangle,\ g_{21}(\alpha_{NS}) = \langle w,\ C(v, v, \bar{v})\rangle,$$

the coefficient $\psi(\alpha_{NS})$, determines the direction of the appearance of the invariant curve can be computed via

$$\psi(\alpha_{NS}) = Re(\frac{e^{i\theta(\alpha_{NS})}g_{21}}{2}) - Re(\frac{(1-2e^{i\theta(\alpha_{NS})})e^{-2i\theta(\alpha_{NS})}g_{20}g_{11}}{2(1-e^{i\theta(\alpha_{NS})})}) - \frac{1}{2}\,|g_{11}|^2 - \frac{1}{4}\,|g_{02}|^2,$$

where $e^{i\theta(\alpha_{NS})} = \lambda(\alpha_{NS})$.
Summarizing the above analysis and using the bifurcation Theory in section 4 in [16], we may state the following theorem.

Theorem 3.2. *If $\psi(\alpha_{NS}) \neq 0$ and the two conditions (3.8), (3.7) are satisfied, then the system (1.2) exhibits a Neimark-Sacker bifurcation at $\alpha = \alpha_{NS} = \dfrac{(\sigma-1)(1+\rho^2)^2}{2\rho(1+b_n\epsilon)}$. Moreover, if $\psi(\alpha_{NS}) < 0$ (respectively, > 0) the Neimark-Sacker bifurcation of system (1.2) at $\alpha = \alpha_{NS}$ is supercritical (respectively, subcritical). In addition, there exists a closed invariant curve that bifurcates from (x^*, y^*) for $\alpha = \alpha_{NS}$.*

4. Chaos control

In this section, the state feedback control method [8, 11, 17] is applied to the system (1.2) to achieve the chaos control. Let (x^*, y^*) be a fixed point of (1.2) and Consider the following controlled form of (1.2)

$$\begin{aligned} x_{n+1} &= \frac{\alpha(1+b_n\epsilon)}{1+x_n^2} + y_n + u_n, \\ y_{n+1} &= y_n - \sigma(x_n - \rho). \end{aligned} \tag{4.1}$$

with the following feedback control law as the control force [11]

$$u_n = -K_1(x_i - x_*) - K_2(y_n - y_*),$$

$k_1,\ k_2$ are the feedback gains.
The Jacobian matrix of the system (4.1) at (x^*, y^*) reads

$$J_c(x^*, y^*) = \begin{pmatrix} \frac{-2\alpha(1+b_n\epsilon)}{(1+\rho^2)^2} - k_1 & 1-k_2 \\ -\sigma & 1 \end{pmatrix}.$$

The characteristic equation corresponding to $J_c(x^*, y^*)$ reads

$$\lambda^2 - tr(J)\lambda + det(J) = 0, \tag{4.2}$$

where $tr(J_c) = 1 - k_1 - \frac{2\alpha(1+b_n\epsilon)}{(1+\rho^2)^2}$ and $det(J_c) = \sigma(1-k_2) - (\frac{2\rho\alpha(1+b_n\epsilon)}{(1+\rho^2)^2} + k_1)$.
Let λ_1 and λ_1 be the roots of (4.2). Then,

$$\lambda_1 + \lambda_2 = 1 - k_1 - \frac{2\alpha(1+b_n\epsilon)}{(1+\rho^2)^2}, \tag{4.3}$$

$$\lambda_1\lambda_2 = \sigma(1-k_2) - k_1 - (\frac{2\rho\alpha(1+b_n\epsilon)}{(1+\rho^2)^2} + k_1). \tag{4.4}$$

The solutions of the equations $\lambda_1 = \pm 1$ and $\lambda_1\lambda_2 = 1$ determine the lines which determine the region of stability stability. Suppose that $\lambda_1\lambda_2 = 1$, then from (4.4) we get

$$l_1\ :\ k_1 = \sigma(1-k_2) - (\frac{2\rho\alpha(1+b_n\epsilon)}{(1+\rho^2)^2} + k_1) - 1. \tag{4.5}$$

Solving (4.3) and (4.4) at $\lambda_1 = 1$ we get

$$l_2\ :\ k_2 = 2. \tag{4.6}$$

Solving (4.3) and (4.4) at $\lambda_1 = -1$, we get

$$l_3\ :\ k_1 = \frac{\sigma(1-k_2)}{2} - (\frac{2\rho\alpha(1+b_n\epsilon)}{(1+\rho^2)^2} + k_1) + 1. \tag{4.7}$$

The three lines $l_1,\ l_2$ and l_3 determine a triangular region in the (k_1, k_2) plane which gives $\mid \lambda_{1,2} \mid < 1$.

5. Numerical simulation

Here, we confirm the obtained theoretical results by performing some numerical simulations. Figure 1 gives some bifurcation diagrams of the system (1.2). Moreover, the maximal Lyapunov exponent corresponding to each bifurcation diagram is introduced below it. In Figure 1 (a), we start with the initial point $(1.5, 0.3)$ with $\epsilon = 0.1,\ \sigma = 0.2,\ \rho = 1.3,\ b_n = -1$. According to Theorem , the system (1.2) undergoes flip bifurcation at $\alpha = 3.4016$ which is illustrated in Figure 1 (a). In Figure 1 (b), we start with the initial point $(-0.8, -1)$ with $\epsilon = 0.1,\ \sigma = 0.5,\ \rho = -1, b_n = -1$. According to Theorem , the system (1.2) undergoes Neimark-Sacker bifurcation at $\alpha = 1.1111$ which is illustrated in Figure 1 (b). In Figure
reffl11 (b), we start with the initial point $(-0.1, -0.1)$ with $\epsilon = 0.2,\ \sigma = 0.3,\ \rho = -0.3, b_n = -1$. According to Theorem , the system (1.2) undergoes Niemark-Sacker

bifurcation at $\alpha = 1.7326$ which is illustrated in Figure 1 (b). Figure 1 (h) illustrates that the system (1.2) undergoes flip bifurcation at $\epsilon = 0.2,\ \sigma = 0.3,\ \rho = 0.3, b_n = (-1)^n,\ \alpha \approxeq 1.7$. Figure 1 (b) illustrates that the system (1.2) undergoes Neimark-Sacker bifurcation at $\epsilon = 0.2,\ \sigma = 0.3,\ \rho = -0.3, b_n = (-1)^n,\ \alpha \approxeq 1.5$. Figure 2 consists of some phase portraits of the system (1.2) associated with Figure

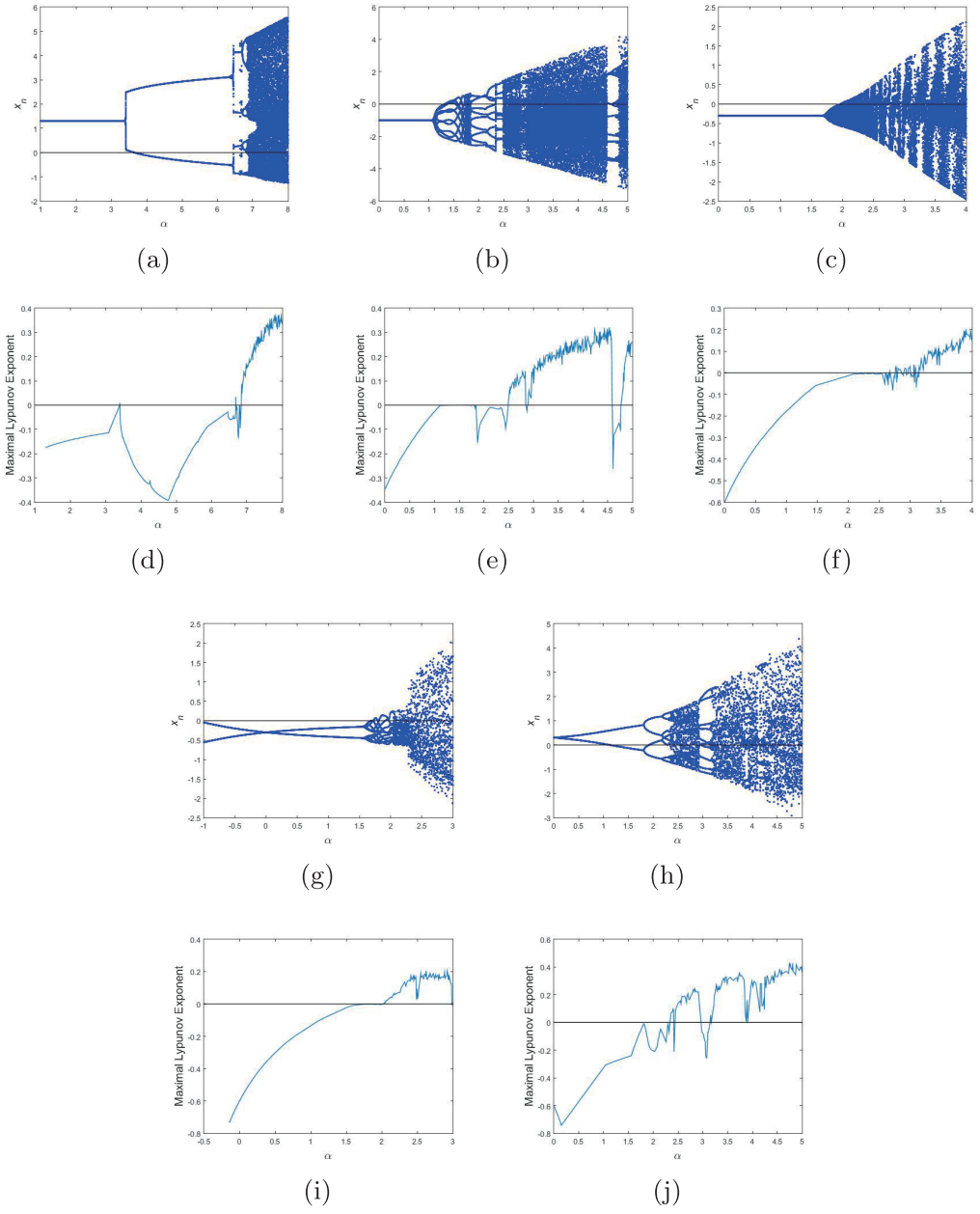

FIGURE 1. Bifurcation diagrams and the corresponding maximal Lyapunov exponent of the system (1.2)

1 (b). In each diagram we use the same values of the parameters which have been used in Figure 1 (b) i.e. $\epsilon = 0.1,\ \sigma = 0.5,\ \rho = -1,\ b_n = -1$ and start with the same initial point $(-0.8,\ -1)$. we can see a smooth invariant circle bifurcates from the fixed point $(-1, -1.45)$, Figure Figure 2 (a), to a circular curve enclosing the fixed point, Figure 2 (b). In Figure 2 (c) and Figure 2 (d), circular curve appears with radius increases as α increases. In Figure 2 (e) the circular curve breakdown. The circular curve appear again, Figure 2 (f). The circular curve breakdown again and a period-9 orbit appears, Figure 2 (g) and Figure 2 (h). Then as α increases the system becomes chaotic, Figure 2 (i). Figure 2 (j) and Figure 2 (k) show that a period-8 orbit appears and the Lyapunov exponent is negative again, Figure 1 (e). Then as α increases the system becomes chaotic as shown in Figure 2 (l), and the Lyapunov exponent is positive again, Figure 1 (e). Figure 3 consists of some phase portraits of the system (1.2) associated with Figure 1 (c). In each diagram we use the same values of the parameters which have been used in Figure 1 (c) i.e. $\epsilon = 0.2,\ \sigma = 0.3,\ \rho = -0.3,\ b_n = -1$ and start with the same initial point $(-0.1,\ -1)$. At $\alpha = 1.7$ the attracting fixed point $(-0.3,\ -1.5477)$ is illustrated in Figure 3 (a). The fixed point loses its stability as α increases, in Figure 3 (b) at $\alpha = 1.74$ and Figure 3 (c) at $\alpha = 1.77$. In Figure 3 (d), Figure 3 (e) and Figure 3 (f) circular curve appears with radius increases as α increases. In Figure 3 (g) the circular curve breakdown at $\alpha = 2.4$. In Figure 3 (h) the closed curve appears again at $\alpha = 2.6$. The curve breakdown at $\alpha = 2.8$, Figure 3 (i), and then as $\alpha \geq 3$ the system becomes chaotic, Figure 3 (j), Figure 3 (k), Figure 3 (l), and the Lyapunov exponent becomes positive, Figure 1 (f). Figure 4 consists of some phase portraits associated with Figure 1 (a). Figure 4 (a) illustrates the the existence of a period-2 orbit. A douple-period bifurcation occurs as α increases and Figure 4 (b) illustrates the existence of a period-4 orbit. Figure 4 (c) illustrates the birth of period-8 orbit. Then, the system becomes chaotic as α increases which is illustrated in Figure 4 (d) and the Lyapunov exponent is positive, Figure 1 (d). Figures 5, 7 and 6 show how a small change in the perturbation parameter ϵ leads to a great change in the qualitative behavior of the system (1.2). As ϵ being the bifurcation parameter, Figure 5 introduces some bifurcation diagrams of the system (1.2) and the corresponding maximal Lyapunov exponent. In Figure 5 (a) we take $\sigma = 0.3,\ \rho = 0.3,\ b_n = -1,\ \alpha = 3$ and start from the initial point $(0.5, -2)$. We can see that when $\epsilon = 0$ i.e. there is no perturbation, the system is chaotic but for small perturbation the system has periodic orbits. Moreover, we can see that a halving-period bifurcation occurs as ϵ increases. The maximal Lyapunov exponent of the system (1.2) corresponding to Figure5 (a) is given in Figure 5 (c). In Figure 5 (b) we take $\sigma = 0.5,\ \rho = -1,\ b_n = -1,\ \alpha = 4$ and start from the initial point $(-0.8, -1.3)$. We can see that a small change ϵ may make the system chaotic or has periodic orbits. The maximal Lyapunov exponent of the system (1.2) corresponding to Figure 5 (b) is given in Figure 5 (d). Figure 6 introduce some phase portraits of the system (1.2) corresponding to Figure 5 (a). In Figure 6 (a), $\epsilon = 0$ the system (1.2) is reduced to the original Rulkov map and it is chaotic as illustrated by the positive value of the maximal Lyapunov exponent in Figure 5 (c). For small perturbation $\epsilon = 0.08$, Figure 6 (b) show that the system no longer chaotic but it has a 4-period and the maximal Lyapunov exponent is negative in Figure 5 (c). Figure

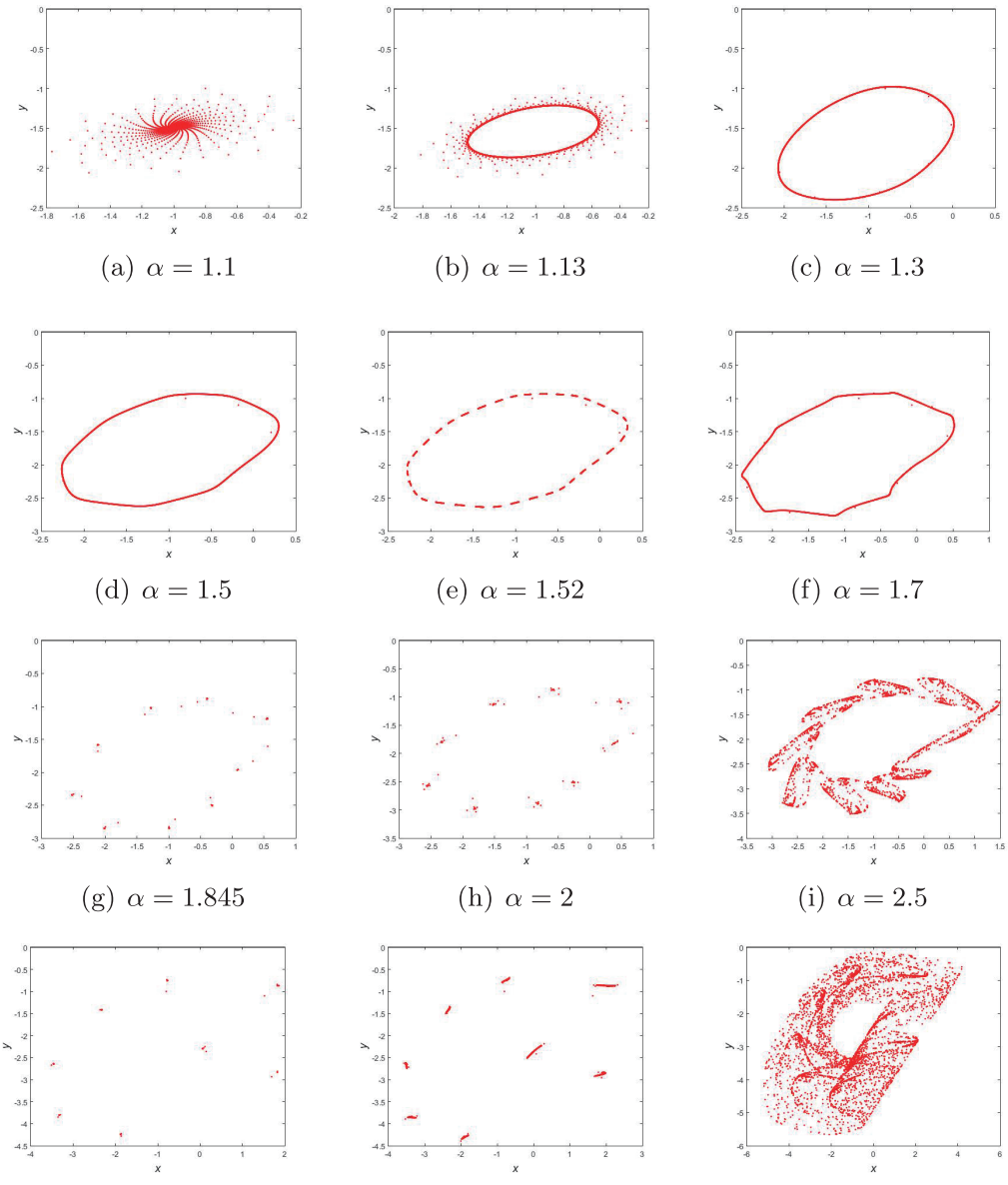

(a) $\alpha = 1.1$ (b) $\alpha = 1.13$ (c) $\alpha = 1.3$

(d) $\alpha = 1.5$ (e) $\alpha = 1.52$ (f) $\alpha = 1.7$

(g) $\alpha = 1.845$ (h) $\alpha = 2$ (i) $\alpha = 2.5$

(j) $\alpha = 4.6$ (k) $\alpha = 4.8$ (l) $\alpha = 4.9$

FIGURE 2. Phase portraits of the system (1.2) associated with Figure 1 (b)

6 (c) show that at $\epsilon = 0.15$ the 4-period is reduced to 2-period. Figure 7 introduces some phase portraits of the system (1.2) corresponding to Figure 5 (b). In Figure 7 (a), $\epsilon = 0$ the system (1.2) is reduced to the original Rulkov map and it is chaotic as indicated by the positive value of the maximal Lyapunov exponent in Figure 5 (d). In Figure 7 (b), there is 8-period at $\epsilon = 0.35$ and the maximal Lyapunov exponent is negative in Figure 5 (d). The system becomes chaotic again in Figure 7 (c) and

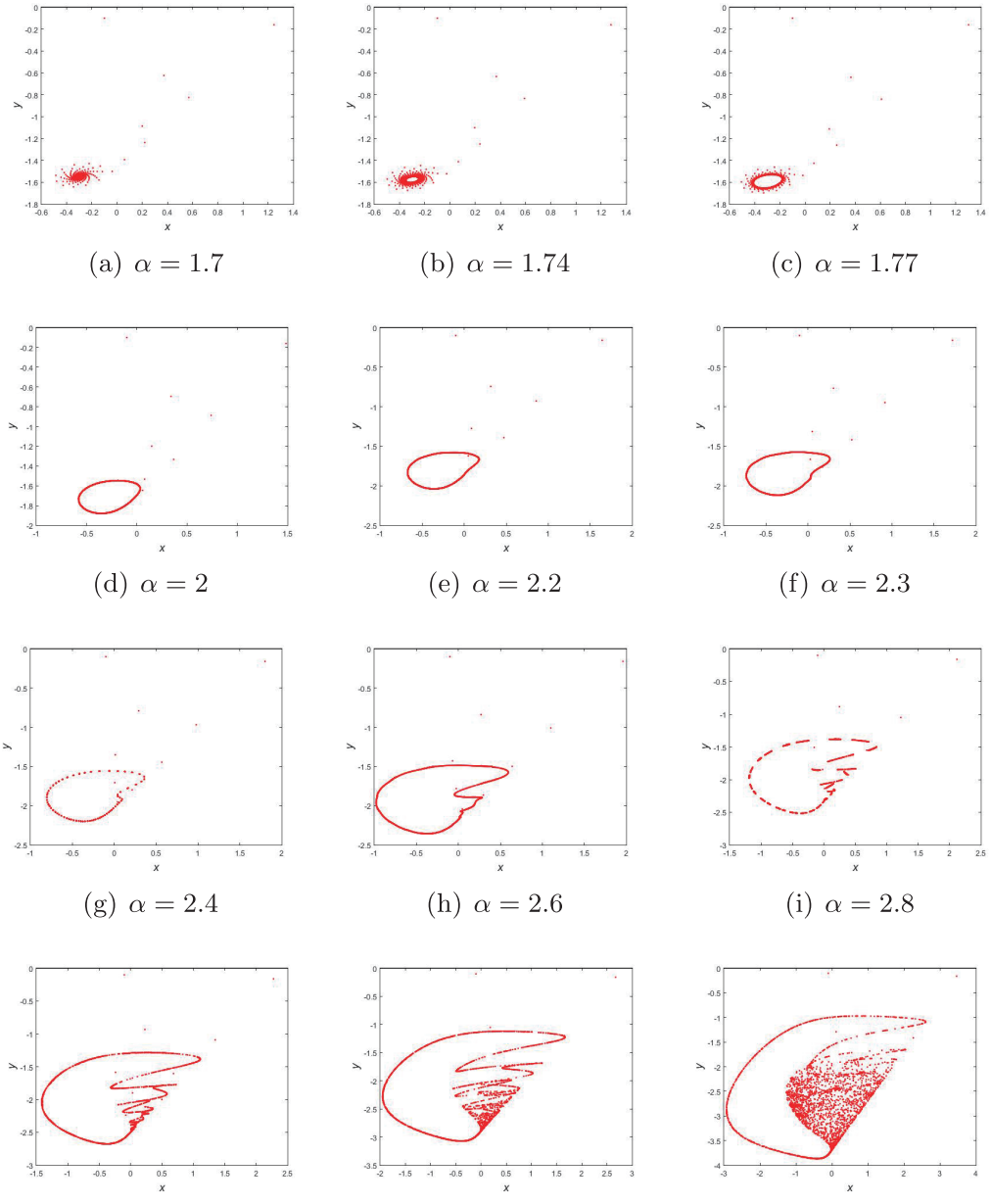

(a) $\alpha = 1.7$ (b) $\alpha = 1.74$ (c) $\alpha = 1.77$

(d) $\alpha = 2$ (e) $\alpha = 2.2$ (f) $\alpha = 2.3$

(g) $\alpha = 2.4$ (h) $\alpha = 2.6$ (i) $\alpha = 2.8$

(j) $\alpha = 3$ (k) $\alpha = 3.5$ (l) $\alpha = 4.5$

FIGURE 3. Phase portraits of the system (1.2) associated with Figure 1 (c)

the maximal Lyapunov exponent is positive in Figure 5 (d). In Figure 7 (d), there is 9-period at $\epsilon = 0.56$ with negative maximal Lyapunov exponent in Figure 5 (d). In Figure 7 (e) and Figure 7 (f), circular curve appears with radius decreases as ϵ increases. Figure 8 shows how the feedback control method works. Figure 8 (a) illustrates the stability region in (k_1, k_2) plan. Figure 8 (b) shows a plot when the

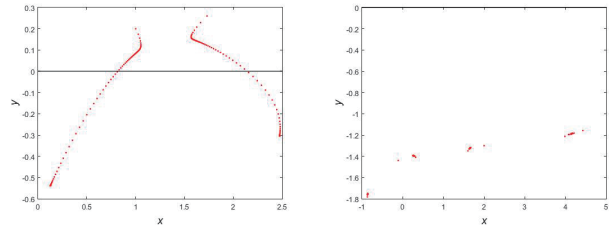

(a) $\alpha = 3.4$ (b) $\alpha = 6.6$

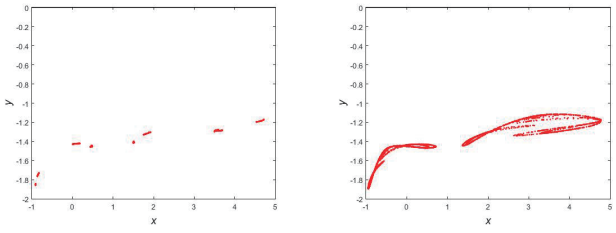

(c) $\alpha = 6.83$ (d) $\alpha = 6.9$

FIGURE 4. Phase portraits of the system (1.2) associated with Figure 1 (a)

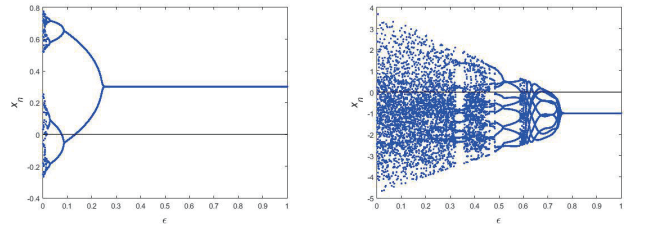

(a) (b)

(c) (d)

FIGURE 5. Bifurcation diagrams and the corresponding maximal Lyapunov exponent of the system (1.2)

control is switched on after 150 iterations and is left switched on. In Figure 8 (c), the control is switched on after 150 iterations and then switched off after the 300th iterate. In Figure 8 (d), the control is switched on after 50 iterations, switched

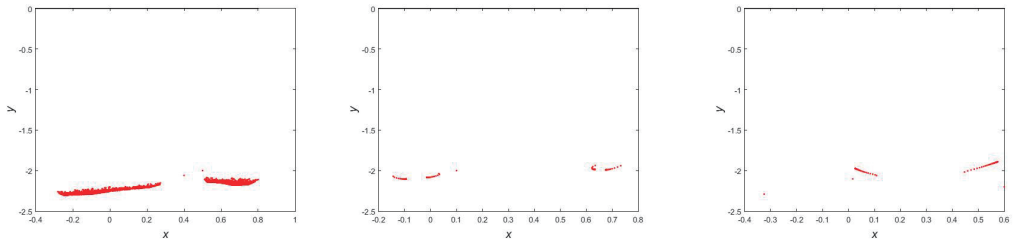

(a) $\epsilon = 0$ (b) $\epsilon = 0.08$ (c) $\epsilon = 0.15$

FIGURE 6. Phase portraits of the system (1.2) corresponding to Figure 5 (a)

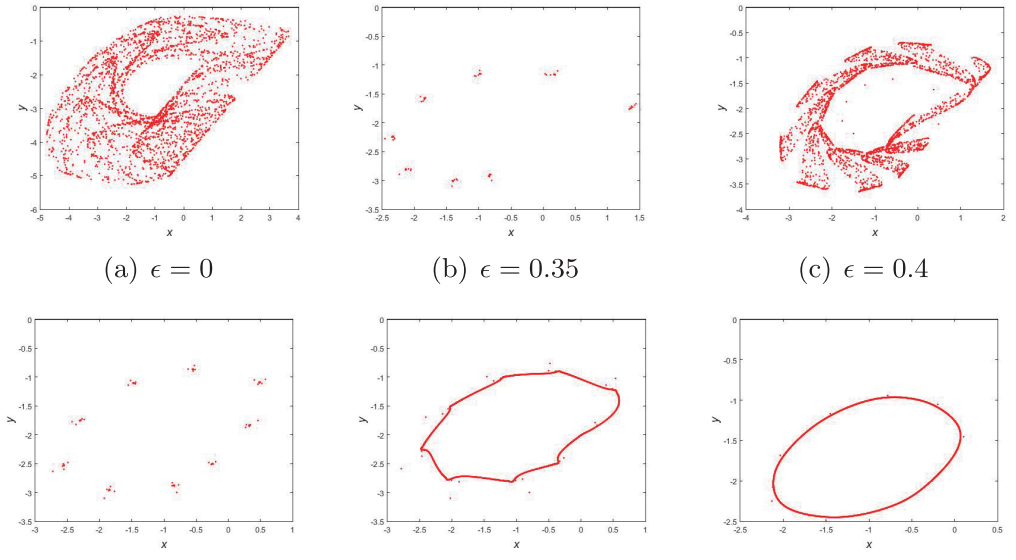

(a) $\epsilon = 0$ (b) $\epsilon = 0.35$ (c) $\epsilon = 0.4$

(d) $\epsilon = 0.56$ (e) $\epsilon = 0.6$ (f) $\epsilon = 0.7$

FIGURE 7. Phase portraits of the system (1.2) corresponding to Figure 5 (b)

off after 200 iterations and then switched on again after 250 iterations and is left switched on.

6. Conclusion

The present study investigates the dynamics of a neuron model that is modified through parametric perturbation in the Rulkov map. The authors carried out a local stability analysis, which demonstrated that the system presents flip bifurcation and Neimark-Sacker bifurcation. To achieve chaos control, the state feedback control approach was employed. Subsequently, numerical simulations were conducted to verify the theoretical outcomes. The research also examines the impact of the perturbation parameter on the system's behavior. Specifically, the findings indicate that even a small perturbation can lead to a significant change in the qualitative

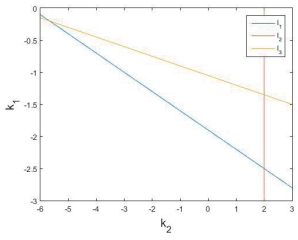

(a) The stability region at $\epsilon = 0.2,\ \sigma = 0.3,\ \rho = 0.3,\ \alpha = 5$

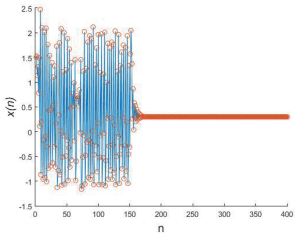

(b) $\epsilon = 0.2, \sigma = 0.3, \rho = 0.3,$ $\alpha = 5,\ k_1 = k_2 = -1$

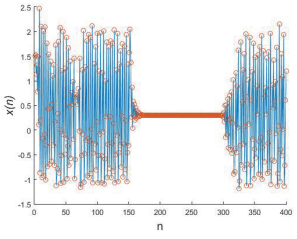

(c) $\epsilon = 0.2, \sigma = 0.3, \rho = 0.3,$ $\alpha = 5,\ k_1 = k_2 = -1$

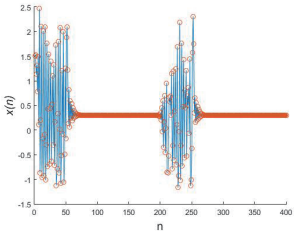

(d) $\epsilon = 0.2, \sigma = 0.3, \rho = 0.3,$ $\alpha = 5,\ k_1 = k_2 = -1$

FIGURE 8. Chaos control of the system (1.2)

dynamics of the system. The system displays multiple periodic orbits, including 4-period, 8-period, and 9-period. Furthermore, by selecting the perturbation parameter as the bifurcation parameter, the study shows that the system may exhibit a halving-period bifurcation.

REFERENCES

[1] C. J. L. Albert, *Regularity and complexity in dynamical systems*, Springer, New York, 2012.
[2] A. V. Andreev, E. N. Pitsik, V. V. Makarov, A. N. Pisarchik and A. E. Hramov, *Dynamics of map-based neuronal network with modified spike-timing-dependent plasticity*, Eur Phys J. **227** (2018), 1029–1038.
[3] D. Biswas and S. Gupta, *Ageing transitions in a network of Rulkov neurons*, Scientific Reports **12** (2022): 433.
[4] H. J. Cao and Y. G. Wu, *Bursting types and stable domains of Rulkov neuron network with mean field coupling*, Int J Bifur Chaos. **23** (2013): 1330041.
[5] T. R. Chay, *Chaos in a three-variable model of an excitable cell*, Physica D. **16** (1985), 233–242.
[6] D. R. Da Costa, M. Hansen and A. M. Batista, *Parametric perturbation in a model that describes the neuronal membrane potential*, Physica A. (2019), 519–525.
[7] G. De Vries, *Bursting as an emergent phenomenon in coupled chaotic maps*, Phys Rev E. **64** (2001): 051914.
[8] S. N. Elaydi, *An Introduction to Difference Equations*, Springer, New York, 1996.
[9] R. FitzHugh, *Impulses and physiological states in theoretical models of nerve membrane*, Biophys J. **1** (1961), 445–466.
[10] J. Guckenheimer and P. Holmes, *Nonlinear Oscillations, Dynamical Systems, and Bifurcations of Vector Fields*, Springer, New York, 1983.
[11] Z. He and X. Lai, *Bifurcation and chaotic behavior of a discrete-time predator-prey system*, Nonlinear Anal. RWA **12** (2011), 403–417.
[12] J. L. Hindmarsh and R. M. Rose, *A model of the nerve impulse using two first-order differential equations*, Nature **296** (1982), 162–164.

[13] A. L. Hodgkin and A.F. Huxley, *A quantitative description of membrane current and its application to conduction and excitation in nerve*, J. Physiol. **117** (1952), 500–544.
[14] B. Ibarz, J.M. Casado and M. A. F. Sanju 卬 n, *Map-based models in neuronal dynamics*, Phys Rep. (2011), 1–74.
[15] E. M. Izhikevich, *Class 1 neural excitability, conventional synapses, weakly connected networks, and mathematical foundations of pulse-coupled models*, IEEE Trans. Neural Netw. **10** (1999), 499–507.
[16] Y. A. Kuzenetsov, *Elements of applied bifurcation Theory*, Springer, New York, 1998.
[17] S. Lynch,*Dynamical Systems with Applications Using MATLAB*, Birkhäuser: Springer, Switzerland, 2014.
[18] C. Morris and H. Lecar, *Voltage oscillations in the barnacle giant muscle fiber*, J Biophys. **35** (1981), 193–213.
[19] C. Robinson, *Dynamical Systems: Stability, Symbolic Dynamics, and Chaos*, CRC Press, Boca Raton, 1999.
[20] N. F. Rulkov, *Modeling of spiking-bursting neural behavior using two-dimensional map*, Phys. Rev. E. **65** (2002): 041922.
[21] N. F. Rulkov, I. Timofeev and M. Bazhenov, *Oscillations in large-scale cortical networks: map-based model*, J. Comput. Neurosci. **17** (2004), 203–223.
[22] G. Tanaka, G. Ibarz, M.A.F. Sanju 卬 n and K. Aihara, *Synchronization and propagation of bursts in a ring of coupled map neurons*, Chaos **16** (2006): 013113.
[23] C. X. Wang and H. J. Cao, *Parameter space of the Rulkov chaotic neuron model*, Commun Nonlinear Sci Numer Simul. **19** (2014), 2060–2070.
[24] C. Wang and H. Cao, *Stability and chaos of Rulkov map-based neuron network with electrical synapse*, Commun Nonlinear Sci Numer Simulat. **20** (2015), 536–545.
[25] H. R. Wilson, *Simplified dynamics of human and mammalian neocortical Neurons*, J. Theor Biol. **200** (1999), 375–388.
[26] S. Winggins, *Introduction to Applied Nonlinear Dynamical Systems and Chaos*, Springer, New York, 2003.
[27] Q. Xu, T. Liu, C. Feng, H. Bao, H. Wu and B. Bao, *Continuous non-autonomous memristive Rulkov model with extreme multistability*, Chin Phys B. **30** (2021): 128702.
[28] Q. Xu, X. Tan, D. Zhu, H. Bao, Y.H. Hu and B.C. Bao, *Bifurcations to bursting and spiking in the Chay neuron and their validation in a digital circuit*, Chaos Solitons Fractals. **141** (2020): 110353.

Manuscript received October 3 2023
revised December 10 2023

A. M. A. El-Sayed
Alexandria, Egypt
E-mail address: amasayed@alexu.edu.eg

S. M. Salman
Alexandria, Egypt
E-mail address: samastars9@alexu.edu.eg

A. M. A. Abo-Bakr
Alexandria, Egypt
E-mail address: ali.abobakr@alexu.edu.eg